

Observations from Preliminary Experiments on
Spatial and Temporal Pressure Measurements
from Near-Field Free Air Explosions

by

Sam E. Rigby, Andrew Tyas, Sam D. Clarke, Stephen D. Fay,
Jonathan J. Reay, James A. Warren, Matt Gant and Ian Elgy

Reprinted from
International Journal of
Protective Structures

Volume 6 · Number 2 · June 2015

Multi-Science Publishing
ISSN 2041-4196

Observations from Preliminary Experiments on Spatial and Temporal Pressure Measurements from Near-Field Free Air Explosions

Sam E. Rigby^{a*}, Andrew Tyas^{a,b}, Sam D. Clarke^a, Stephen D. Fay^{a,b}, Jonathan J. Reay^b, James A. Warren^{a,b}, Matt Gant^c and Ian Elgy^c
^aDepartment of Civil & Structural Engineering, University of Sheffield, Mappin Street, Sheffield, S1 3JD, UK
^bBlastech Ltd., The BioIncubator, 40 Leavygreave Road, Sheffield, S3 7RD, UK
^cDefence Science and Technology Laboratory (DSTL), Porton Down, Salisbury, Wiltshire, SP4 0JQ, UK

Received on 20 December 2014; Accepted on 9 March 2015

ABSTRACT

It is self-evident that a crucial step in analysing the performance of protective structures is to be able to accurately quantify the blast load arising from a high explosive detonation. For structures located near to the source of a high explosive detonation, the resulting pressure is extremely high in magnitude and highly non-uniform over the face of the target. There exists very little direct measurement of blast parameters in the near-field, mainly attributed to the lack of instrumentation sufficiently robust to survive extreme loading events yet sensitive enough to capture salient features of the blast. Instead literature guidance is informed largely by early numerical analyses and parametric studies. Furthermore, the lack of an accurate, reliable data set has prevented subsequent numerical analyses from being validated against experimental trials.

This paper presents an experimental methodology that has been developed in part to enable such experimental data to be gathered. The experimental apparatus comprises an array of Hopkinson pressure bars, fitted through holes in a target, with the loaded faces of the bars flush with the target face. Thus, the bars are exposed to the normally or obliquely reflected shocks from the impingement of the blast wave with the target. Pressure-time recordings are presented along with associated Arbitrary-Lagrangian-Eulerian modelling using the LS-DYNA explicit numerical code. Experimental results are corrected for the effects of dispersion of the propagating waves in the pressure bars, enabling accurate characterisation of the peak pressures and impulses from these loadings. The combined results are used to make comments on the mechanism of the pressure load for very near-field blast events.

Key words: blast, experiment, hopkinson pressure bar, near-field, validation

*Corresponding author. Tel.: + 44 (0) 114 222 5724. E-mail address: sam.rigby@sheffield.ac.uk

1. INTRODUCTION

When a blast wave strikes a target the resulting pressure imparted by the blast can be in the order of several megapascals acting over microsecond to millisecond durations. Experimental quantification of the blast load arising from a high explosive detonation has been a topic of interest since the mid-1940s (see Esparza [1] for a detailed review), with the well-known Kingery and Bulmash [2] semi-empirical predictions forming the basis of design guidance in the literature, such as the UFC-3-340-02 design manual [3], the ConWep computer code [4] and the LOAD_BLAST [5] module of LS-DYNA [6]. These semi-empirical predictions are based on the compilation of a number of large-scale blast trials, parametric studies and early numerical simulations, and have been shown to match closely controlled experimental tests with remarkable accuracy for far-field events [7–11].

If the blast is located close to the target, however, the interaction between blast wave and structure and hence the imparted load is more complex. Near-field events are typically characterised by extremely high magnitude, highly spatial and temporally non-uniform loads (see Figure 1) and are associated with scaled distances, Z , less than $\sim 1 \text{ m/kg}^{1/3}$, where $Z = R/W^{1/3}$, R is the distance from the centre of the explosive, and W is the charge mass expressed as an equivalent mass of TNT. Here, the difficulties associated with controlling the test parameters have a greater impact on the test-to-test repeatability and as such the semi-empirical predictions are less accurate [12]. Furthermore, robust instrumentation is required to measure the extreme pressures associated with near-field loading. At scaled distances $Z < 0.4 \text{ m/kg}^{1/3}$, direct measurements of the blast parameters are either non-existent or very few [1] and the semi-empirical predictive data for this range is based almost entirely on parametric studies.

Previous researchers, therefore, have primarily relied on numerical modelling approaches to simulate the detonation, air-shock propagation and shock-structure interaction in the near-field. From these studies, authors have been able to research the complex interaction between the shock wave and expanding detonation products [14], scaled-distance relationships for near-field explosions [15], the limits of representing the explosive as an ideal gas [16], mesh sensitivity effects [17] and the complex 3D waveform of an expanding shock wave [18]. Despite these valuable observations, little definitive, well controlled experimental data is offered to validate such numerical modelling. Owing to the extremely onerous conditions near to the source of the explosion, close-in experimental blast parameter measurements are typically conducted by

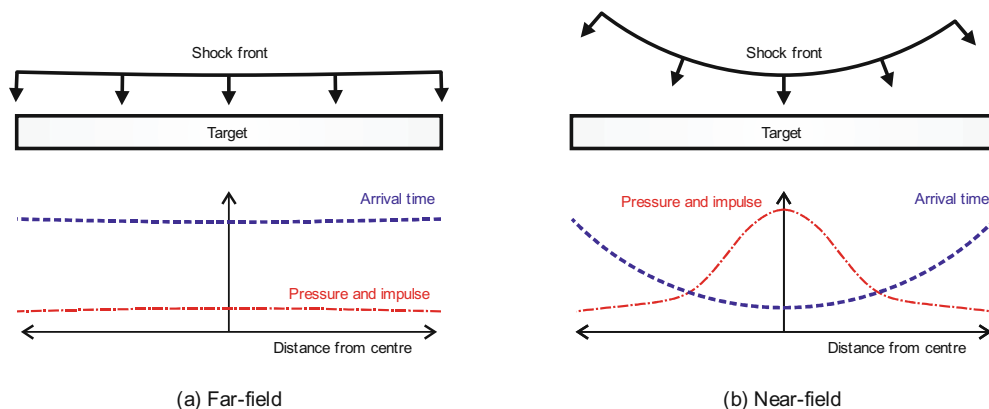


Figure 1. Blast interaction diagram and loading parameters associated with (a) far-field and (b) near-field blast loading (13)

measuring the residual momentum – and hence inferring the imparted impulse – of a small, rigid metal plug embedded within a larger target surface [19, 20]. The impulse plug method has been shown to reduce test-to-test scatter and gives an indication of the imparted load at discrete points on the target. What the method does not offer, however, is sufficient temporal resolution of the applied blast overpressure, which is a necessary requirement in order to discern the mechanism of near-field loading scenarios and to provide data for stringent validation.

Recently, a large scale experimental approach to the direct measurement of the spatial and temporal variation in loading resulting from an explosive event has been developed [13, 21–22]. This experimental approach utilises a fixed target plate through which Hopkinson pressure bars (HPBs) are inserted, and allows the overpressure-time histories for an array of bars to be generated, giving the spatial and temporal distribution of blast overpressure acting on a rigid target. This paper presents initial results from experiments conducted as part of the commissioning phase of the apparatus, alongside associated Arbitrary-Lagrangian-Eulerian modelling using the LS-DYNA explicit numerical code [6]. The combined results described herein will provide useful insights into the mechanism of loading for extremely close-in detonations, and will provide data to inform further study on near-field blast loading.

2. EXPERIMENTAL WORK

An experimental methodology has been developed to capture data from extremely aggressive blast events, such as shallow-buried land mines and near-field bare explosive charges. This necessitated the fabrication of a purpose-built testing apparatus. The testing apparatus consists of two steel fibre and bar reinforced concrete frames spaced 1 m apart, with each frame comprising two 500 mm square columns with a 750 mm deep, 500 mm wide concrete beam spanning between the two columns. A 50 mm thick steel ‘acceptor’ plate was cast into the underside of each of the beams to allow a 1400 mm diameter, 100 mm thick mild steel target plate to span underneath. A central 10.5 mm hole was drilled through the thickness of the target plate with subsequent holes at 25 mm spacing (centre to centre) parallel and perpendicular to the span of the concrete beams. 10 mm diameter, 3.25 m long EN24(T) steel Hopkinson pressure bars (HPBs) were inserted through the bar holes and suspended (from a receiver frame placed atop the main reaction frame) such that their ends sat flush with the target face, as can be seen in Figure 2. Up to 17 bars used can be located within a 100 mm radius circle centered above the charge location, with the ability to load subsequent bars at any distance up to 250 mm away from the target centre.

Perimeter-mounted semiconductor strain gauges were located 250 mm from the loaded face of the bars. An axial stress pulse beginning at the loaded face and propagating along the length of the bar will cause a change in strain at the perimeter as it propagates over the gauge location, hence the strain gauges can be used to measure the temporal variation of blast overpressure acting at discrete points on the target face. An in-house interpolation routine [22] enables a detailed description of the spatial variation of blast to be inferred from the array of overpressure-time readings. For the preliminary testing reported in this paper, one central HPB was located directly in line with the centre of the charge (bar 5) with four bars (bars 1–4) located at 100 mm distance away from the central bar, as is shown in Figure 3. These bars are referred to as ‘normal’ and ‘radial’ bars respectively.

Strain data was recorded using a 14-Bit digital oscilloscope at a sample rate of 1.56 MHz, triggered via a voltage drop in a breakwire embedded in the charge periphery to synchronise the recordings with the detonation. A small sacrificial timber sling was hung underneath the target plate for each test to hold the charge in position (see Figure 2). The detonator was placed up through a hole in the timber sling into the bottom of the charge, as a preliminary

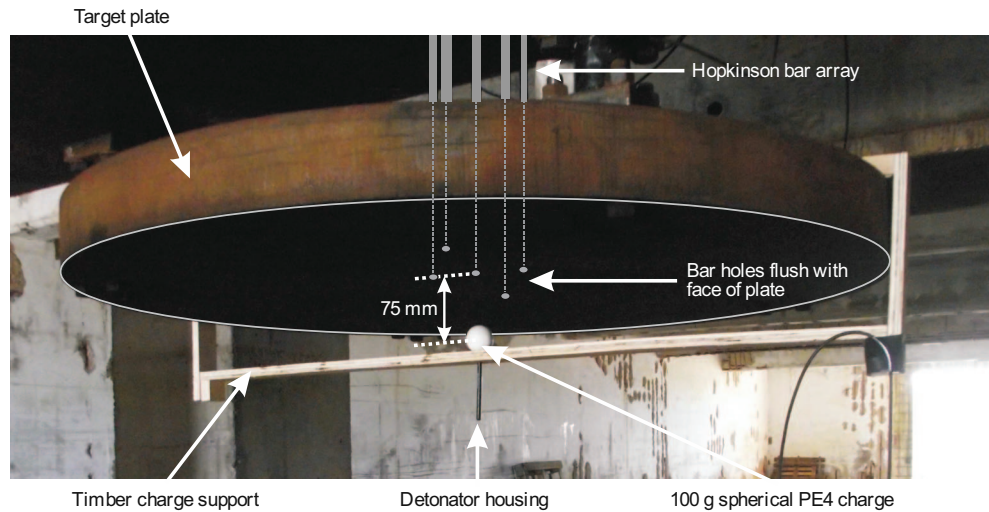


Figure 2. Photograph of test arrangement

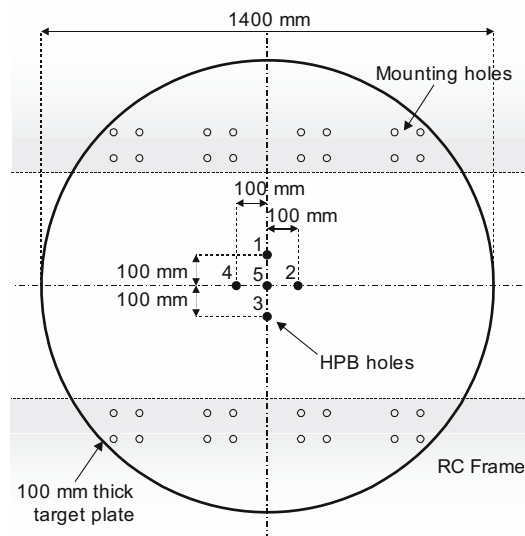


Figure 3. Detail of the target plate with central (5) and radial bars (1, 2, 3, 4) used in this study

study showed that this arrangement is preferential over a top-inserted detonation because of the risk of the signal cable or breakwire coming into contact with the face of one of the bars and contaminating the data [22]. The timber charge support was selected to facilitate quick experimental turnaround and consistent charge placement, and whilst not entirely indicative of free-air loading, the reflection from the timber sling is expected to have a minor influence on the data. In order to more definitively capture free-air detonation physics, recent work has moved towards a less invasive system, however the results presented in this paper still offer valuable insights into the mechanism of near-field blast loading.

Six tests were conducted in total, with 100 g spherical PE4 charges detonated at 75 mm normal distance from the centre of the charge to the bottom of the plate (as in Figure 2), giving a scaled distance of $0.15 \text{ m/kg}^{1/3}$ for the normal bar, and a scaled distance of $0.25 \text{ m/kg}^{1/3}$ and an angle of incidence of 53° for the radial bars. The first three charges were detonated with non-electric EuroNel In-Hole detonators with an NEQ of 0.9 g, made up of 0.3 to 0.35 g Lead Azide Priming Charge with the remaining NEQ made up of a low density PETN. Tests four to six were detonated with medium intensity DaveyDet electrical detonators with an NEQ of 0.8 g PETN.

3. NUMERICAL MODELLING

An Arbitrary-Lagrangian-Eulerian (ALE) analysis was conducted using the LS-DYNA explicit numerical code [6]. LS-DYNA solves the ALE governing equations of conservation of mass, momentum and energy in two steps known as an operator split. Firstly, the solution is advanced in time by evaluating the state variables in a Lagrangian framework where the mesh is attached to and deforms with the material it is representing. Secondly, the mesh is transported back to its original un-deformed position in an Eulerian framework as the state variables are transported across element boundaries. This process is then repeated until the termination time is reached. The physics of the problem are treated in the Lagrangian phase, while the advection phase is entirely computational. The ALE method has particular application for the simulation of high explosive events because weaknesses such as excessive mesh deformation (entanglement, instabilities and decreasing time step size) associated with Lagrangian solvers, and problematic treatment of mixing and material interfaces associated with Eulerian solvers are eliminated or better treated in the numerical model [23]. This study uses the Van Leer advection method with half-index shift [24], which is generally recommended for high explosive problems [6].

The air was modelled using the EOS_LINEAR_POLYNOMIAL equation of state (EOS)

$$p = C_0 + C_1\mu + C_2\mu^2 + C_3\mu^3 + (C_4 + C_5\mu + C_6\mu^2) E \quad (1)$$

where $C_0, C_1, C_2, C_3, C_4, C_5$ and C_6 are constants, $\mu = \rho/\rho_0 - 1$, ρ and ρ_0 are the fluid density and initial density, and E is the specific internal energy (energy per unit volume). If the variables C_0, C_1, C_2, C_3 and C_6 are all set to equal 0, and C_4 and C_5 are set equal to $\gamma - 1$, where γ is the ratio of specific heats ($\gamma = 1.4$ for air), the equation reduces to the familiar ideal gas equation of state

$$p = (\gamma - 1) E \rho / \rho_0 \quad (2)$$

The air was modelled using the MAT_NULL material model, with material model and EOS parameters shown in Table 1. A specific internal energy, $E = 253.4 \text{ kPa}$, was given to set the atmospheric pressure to 101.36 kPa .

The explosive was modelled with MAT_HIGH_EXPLOSIVE_BURN material model and Jones-Wilkins-Lee (JWL) semi-empirical equation of state, EOS_JWL [25]. The density, ρ , detonation velocity, D , and Chapman-Jouguet pressure, PCJ , of the explosive are defined in the material model and the pressure, volume, energy relation of the explosive is given as

$$p = A \left(1 - \frac{\omega}{R_1 V} \right) e^{-R_1 V} + B \left(1 - \frac{\omega}{R_2 V} \right) e^{-R_2 V} + \frac{\omega E}{V} \quad (3)$$

where A, B, R_1, R_2 and ω are constants, V is the volume and E is the internal energy. The parameters for PE4 are also shown in Table 1. PE4 is nominally identical to C4; hence the parameters used in this study were taken from the values for C4 published by

Table 1. Material model and equation of state parameters for air and PE4 (SI units). Parameters for PE4 are taken from the values for C4 published by Dobratz & Crawford (26)

	MAT_NULL							
Air	ρ_0	1.225						
	EOS_LINEAR_POLYNOMIAL							
	C_0	C_1	C_2	C_3	C_4	C_5	C_6	E_0
	0.0	0.0	0.0	0.0	0.4	0.4	0.0	253.4E3
	MAT_HIGH_EXPLOSIVE_BURN							
PE4	ρ_0	D	PCJ					
	1601	8193	2.80E10					
	EOS_JWL							
	A	B	R_1	R_2	ω	E_0		
	609.8E9	12.95E9	4.50	1.40	0.25	9.0E9		

Dobratz & Crawford [26]. Modelling the air and explosive separately enables potential effects such as interaction at the air/explosive interface to be studied.

It has been shown that owing to a second-order advection error in LS-DYNA, transport of material diagonally through elements can result in numerical oscillations, energy losses and lower fidelity simulations [27]. For this study the analysis was initiated using 2D axisymmetric ALE elements in a radially symmetric mesh, which was then re-mapped onto a rectangular mesh using the INITIAL_ALE_MAPPING feature in LS-DYNA [28]. The information was re-mapped immediately before impinging on the target, at $t = 11\mu\text{s}$, to allow for the nominally rigid target to be modelled using nodal point constraints, ensuring that the blast wave arrived spherically symmetric whilst also simplifying the modelling of the reflecting surface [27]. Energy is conserved through this process even when re-mapping onto meshes up to 20 times coarser than the original mesh [29]. The 100 g PE4 explosive was modelled with a radius of 24.61 mm. The radially symmetric mesh comprised 506,800 elements with a largest element length of 0.3 mm, and the rectangular mesh comprised 833,500 elements, all with a side length 0.15 mm. A domain of 0.075×0.25 m was specified to prevent expansion waves from the domain edges contaminating the results during the analysis [30].

Numerical information was recorded at locations corresponding to the placement of the experimental pressure bars (directly above the centre of the charge, and 100 mm horizontal distance along the target face away from the charge centre) and also in x and y arrays (detailed in the following section) using the DATABASE_TRACER feature in LS-DYNA. For these locations, the gauges were specified to remain at a fixed co-ordinate. A final gauge was specified at the extreme top edge of the explosive, and was set to track that material point, i.e. storing the location of the air/explosive interface. Validation of LS-DYNA for modelling blast events is provided in Ref. [31].

4. RESULTS

Figure 4 shows the overpressure-time histories recorded by the normal (bar 5) and radial Hopkinson bars (1, 2, 3 and 4). The time data of the experimental signals were shifted to account for the arrival time of the blast wave and transit time of the stress pulse from the

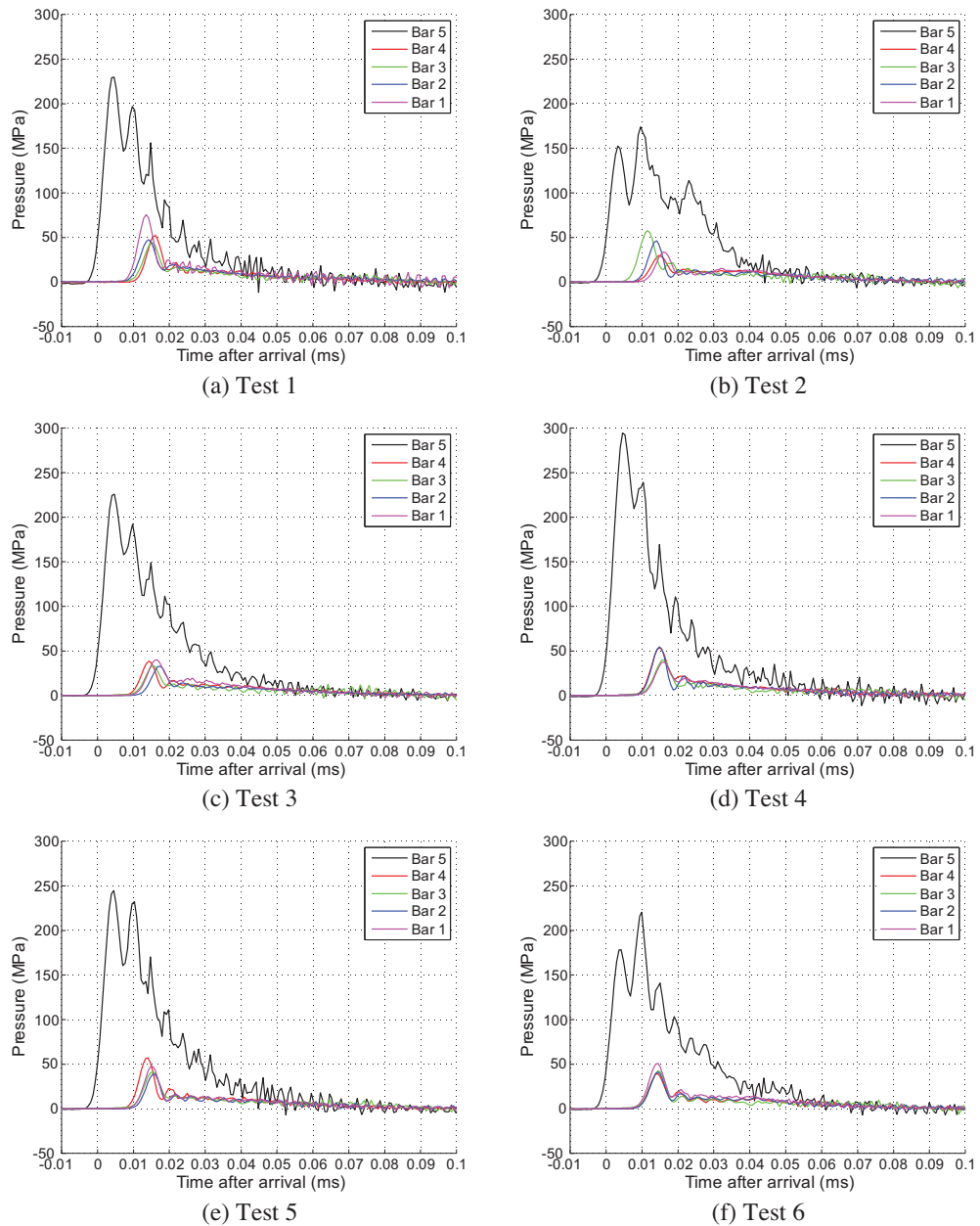


Figure 4. Experimental overpressure-time histories

front face of the bar to the gauge location, i.e. $t = 0$ corresponds to the beginning of the pressure trace for bar 5 (with dispersive effects appearing to cause smoothing at the head of the pulse). The relative times between the normal and radial bar signals were maintained. Figure 5 shows the impulse-time histories given by numerically integrating the recorded overpressure-time signals with respect to time.

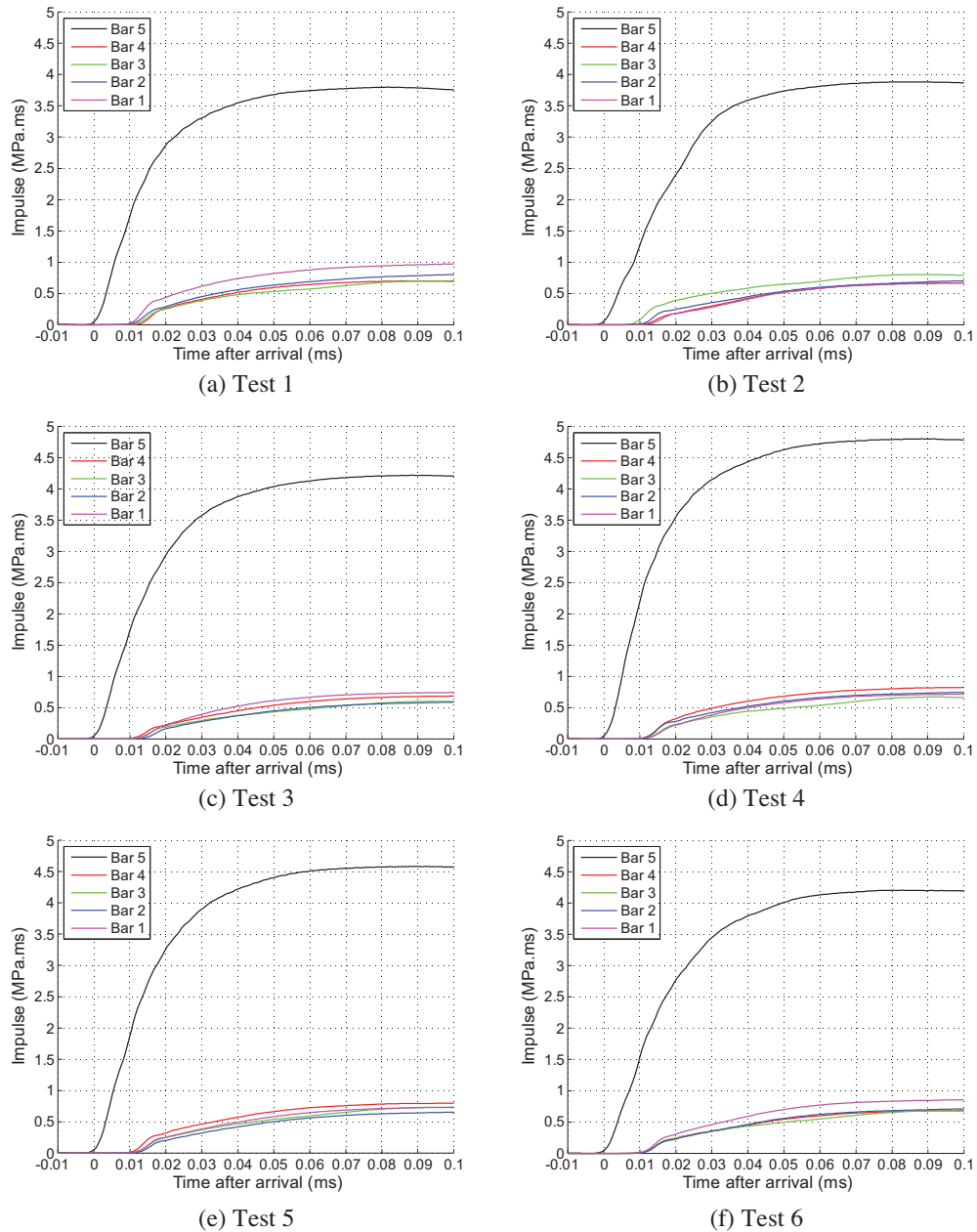


Figure 5. Experimental impulse-time histories

As a stress pulse propagates along a cylindrical bar, each Fourier frequency component will travel with a different velocity, which causes the well-known Pochhammer-Chree dispersion. The result of this is, for a signal recorded at some distance along the bar, certain frequencies will have fallen out of sync. This can be seen clearly by the oscillatory nature of the experimentally recorded pressure signals. Frequency domain phase-shift methods are not

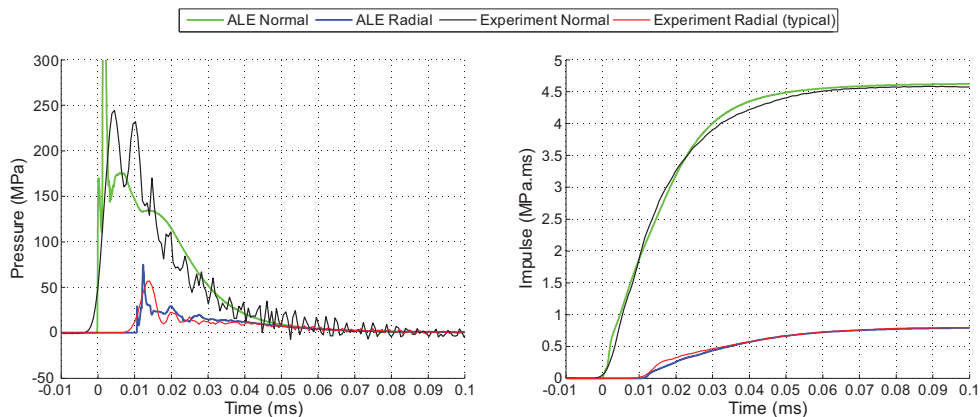


Figure 6. (a) Numerical overpressure-time history and (b) impulse-time history. Experimental recordings from test 5 are shown for comparison

considered at this stage and instead the results are presented ‘as recorded’, however the implication of Pochhammer-Chree dispersion will be discussed in subsequent sections.

Typically the experimental peak overpressures (Figure 4) all lie within the range of 220–290 MPa for the normal bar, and consistently around 50 MPa for the radial bars, with the exception of test 2 (Figure 4(b)), which appears to have been subjected to either an incomplete detonation or slightly non-central charge placement. The impulses (Figure 5) range between 3.8–4.8 MPa.ms for the normal bar and between 0.6–1.0 MPa.ms for the radial bars. There appears to be a small increase in impulse when using a Davey electrical detonator, however this effect is only noticeable for the normal bar location, suggesting the detonator type slightly increases the directionality of the blast but has little effect on the total energy release. The relative arrival time of the radial bars is extremely consistent between tests, and also for each HPB location within any given test, typically arriving between 8 and 10 μs after the shock wave arrives at the normal bar. This suggests that a high level of experimental control is being achieved, and the expansion of the detonation products and resulting shock wave is largely spherically symmetric.

Figure 6 shows the ALE overpressure-time and impulse-time histories at the bar locations alongside the experimental results of bar 5 and bar 4 from test 5 for comparison. The numerical results were time-shifted to match the time-base of the experimental recordings.

5. ALE NEAR-FIELD LOADING MECHANISM

The ‘modified Friedlander’ [32] exponential decay is known to accurately represent the overpressure-time function of blast loads in the medium to far-field [9], however the form of the blast pressure may be over-simplified by assuming a regular decay from peak overpressure over the positive phase duration for close-in explosions. It is clear that the blast overpressure in Figure 6(a) does not comprise a regular transient decay but rather exhibits more complex behaviour. Figure 7 shows a repeat of the normally reflected numerical overpressure-time history from the ALE analysis. Two features to note, which become the focus of the remainder of this section, are annotated in Figure 7 and represent reflection off the air/explosive contact interface and reduction in pressure caused by localised clearing.

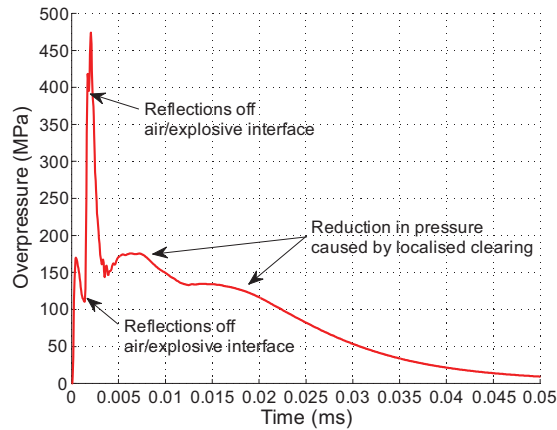


Figure 7. Numerical overpressure-time history at the centre of the plate with features annotated

5.1. AIR/EXPLOSIVE INTERFACE

Edwards et al. [14] proposed a model based on interaction of the reflected pressure wave and the contact interface between the air and explosive to account for the blast pressure profiles observed in their experimental trials. Verification of this interaction model was provided by means of a 1D Lagrangian analysis, however the numerical simulations (conducted in 1992) were not of sufficient resolution to allow for quantitative comparison and were instead only provided as a means for qualitative discussion. It is perhaps because of a lack of clear evidence that this interaction model is not well established in the current literature. The ALE results in Figure 7 show the arrival of the first shock wave with a peak magnitude of 170 MPa. Following this, two secondary shock waves of similar magnitude arrive shortly after, and the peak overpressure rises to around 475 MPa. This behaviour agrees with the model proposed by Edwards et al. and can be further explored.

Figure 8(a) shows a fringe plot of the overpressure-time history for an array of gauge locations in line with the centre of the charge. The co-ordinate origin is located in the centre of the charge, i.e. $y = 0.075$ m gives the conditions at the target centre and lower values of y indicate points in space in front of the target. As discussed by the current authors in Ref. [27], acceleration-time plots effectively show the location of the shock front with respect to time. In Figure 8(b), the vertical particle acceleration-time is shown for the same gauge locations. The direction of the acceleration can be used to investigate the mechanism of loading for extremely close-in blast events. In both diagrams, the dashed black line indicates the expanding contact interface between the air and the explosive products.

In Figure 8(a), the reflection of the primary shock can be seen travelling downwards from the centre of the target at approximately 2,000 m/s (the reflection of the shock front travels from $y = 0.075$ m to $y = 0.073$ m in approximately $1 \mu\text{s}$). This reflection causes an increase in air pressure, and is acting as a compressive wave as the particle acceleration is in the same direction (downwards) as the direction of travel of the shock wave [27]. Just prior to $1 \mu\text{s}$ after the arrival of the blast wave, this reflection of the primary shock wave encounters the interface between the expanding detonation products and the air. An impedance mismatch between the two gasses causes the shock wave to reflect off the interface, again as a compressive wave and again causing an increase in pressure. This reflected shock front

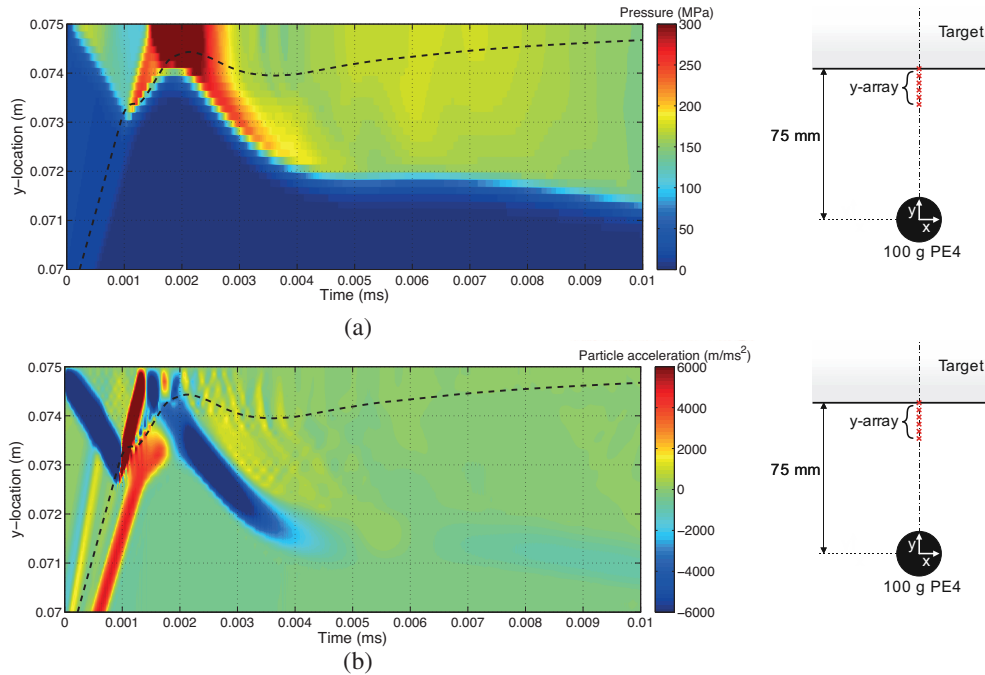


Figure 8. Fringe plots of (a) overpressure and (b) vertical particle acceleration versus time for positions aligned vertically above the centre line of the charge. The dashed black line indicates the interface between air and explosive

travels marginally faster (indicating a higher pressure) and arrives at the target at around $1.5 \mu\text{s}$. Successive reflections off the rigid target and air/explosive interface can be seen, with another reflection arriving at the target at around $1.8 \mu\text{s}$. With each reflection, part of the wave is transmitted into the detonation products, particularly as the air is continually being compressed by these oscillating waves and hence increasing in pressure. The oscillations appear to dampen out shortly after $2.0 \mu\text{s}$, whereby the blast overpressure begins a more regular temporal decay. Interestingly, the arrival of the first reflection with the interface, at $1.0 \mu\text{s}$, is of sufficient magnitude to cause the interface to temporarily deflect away from the target, before continuing to expand outwards.

A compressive wave can be seen propagating through the detonation products, just behind the contact interface. This may be evidence of the well-known ‘second shock’, seen in far-field trials [32]. This gradually impinges on the interface as it is travelling with a similar velocity and hence does not feature as a noticeable second shock for this scaled distance, and is not particularly discernible from the successive primary shock reflections off the air/explosive interface.

5.2. LOCALISED CLEARING

When a plane blast wave strikes a target of finite lateral extent, an instantaneous imbalance between the higher reflected pressure on the front face of the target and the lower incident pressures on the side wall of the target causes diffraction of the blast wave around the target edge [33]. This diffraction wave is driven by the pressure imbalance which sets up flow around the target edge as the higher pressure gas moves towards the lower pressure regions

around the target periphery. This effect is known as ‘clearing’ of the blast wave. Whilst it is known that blast wave clearing can have a significant influence on the response of deformable targets to far-field blast loads [34, 35], it is typically neglected in the near-field due to the fact that the reflected pressure acting on the centre of the target has usually ceased before the arrival of the clearing wave from the target edges [36].

In near-field loading, as angle of incidence effects and scaled slant distances increase across the target face, large differences in pressure develop with the magnitude of the blast pressure rapidly decreasing with increasing distance away from the centre of the target. This sets up the conditions for localized blast wave clearing to occur.

Whilst this clearing mechanism is similar to traditional clearing in that it involves movement of air from higher to lower regions of pressure, it differs in the fact that it begins in the centre of the target and propagates outwards, suggesting that localised clearing begins *immediately* on arrival of the blast wave rather than beginning only once the blast wave has reached an extreme edge of the reflecting surface. Furthermore, there will be no point on the target where there is an instantaneous imbalance between the pressures, and instead there will be a gradient across the entire face of the target. Because of this, rather than definitive shock fronts propagating across the loaded face as per Ref. [27] and Figure 8(a), one should expect to see gradual particle motion away from the target centre. This behaviour would not have been witnessed in the work by Edwards et al. [14] because the analysis was conducted in 1D only.

Figure 9(a) shows a fringe plot of the overpressure-time history for an array of gauge locations, aligned horizontally along the face of the target with $x = 0$ m corresponding to the location of the target centre. Rather than showing a shock front distance-time diagram for

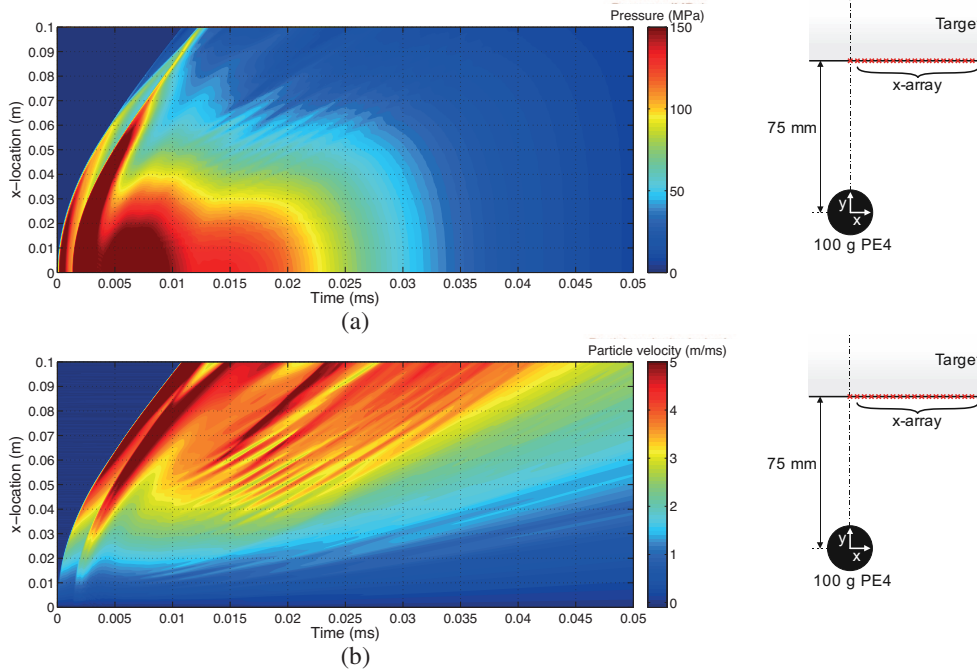


Figure 9. Fringe plots of (a) overpressure and (b) horizontal particle velocity versus time for positions aligned horizontally along the target face

reasons outlined previously, Figure 9(b) shows horizontal velocity-time for the same gauge locations, i.e. the particle velocity along the target face and away from the target centre only.

After the arrival of the blast wave, there is a sustained period of higher pressure behind the shock front near the centre of the target, as is shown in Figure 9(a). This is gradually ‘cleared’ by a region of high velocity that travels outwards from the target centre and causes the development of large horizontal velocities – the effect of which is particularly pronounced from 0.05 m outwards. This large velocity is sustained for some 25–30 μs , whereby the pressure begins to act more uniformly across the centre of the target. The fact that the higher horizontal velocities are acting in regions of lower pressure is indicative of the mechanism of clearing. This differs from the relatively short period where higher velocities and pressures are concurrent – this is caused by radial expansion of the shock front, and ceases almost immediately after the arrival of the shock front, largely before any clearing effects take place. It appears that a velocity gradient gradually establishes across the target face during the late-time behaviour of the blast load. The clearing velocity should be expected to increase with distance from the centre of the target plate due to the cumulative velocity increase from the pressure imbalances, which is captured well by the numerical model. The clearing velocity decreases with time due to both the temporal decay of the blast pressure and pressure equalisation from the effects of clearing.

6. DISCUSSION

With knowledge of the mechanism of near-field loading according to the numerical analysis, it is now possible to examine the experimental recordings for such features and comment on the agreement between experiment and numerical results. Figure 10 shows the peak impulse from all experimental tests and all bar locations compared to the numerical model. The experimental recordings demonstrate good repeatability and the numerical model is able to predict the impulse recorded at the normal and oblique points to a high level of accuracy. This recorded impulse is not significantly affected by dispersion of the stress pulse [37].

Because the temporal as well as spatial distribution of pressure has been recorded, a more stringent validation of the numerical model can be undertaken. This, however, requires the recorded pressure signals to be corrected for the Pochhammer-Chree dispersion effects discussed previously. Figure 11 shows ALE and dispersion corrected experimental pressure-time histories for the normal and radial HPB locations. ConWep [4] predictions are also shown for reference.

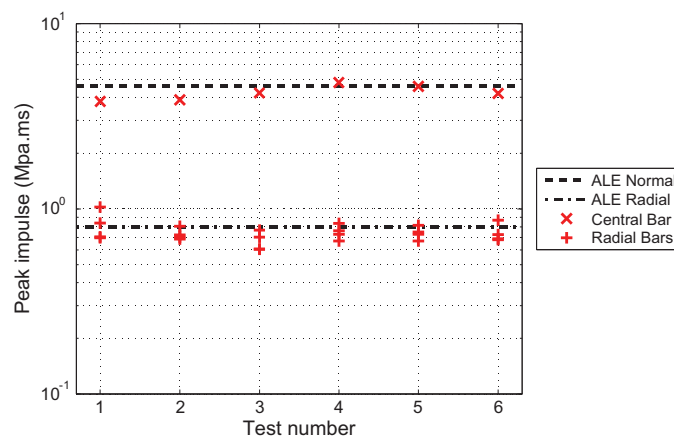


Figure 10. Numerical and experimental peak impulses

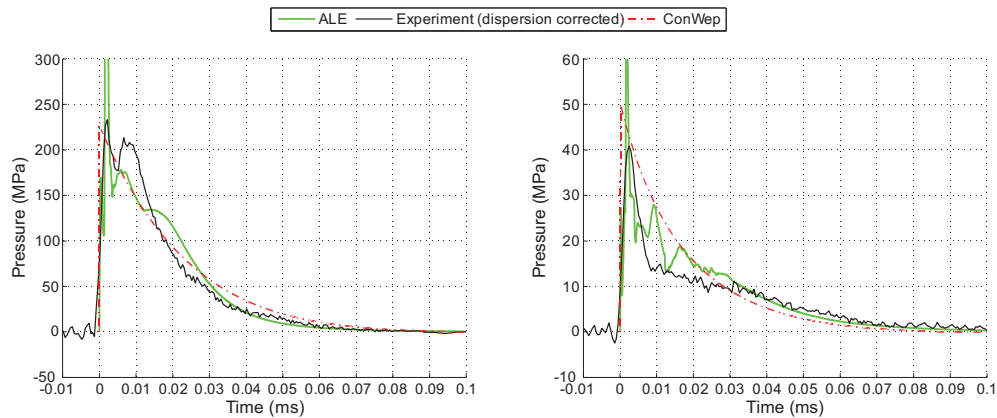


Figure 11. (a) Normally reflected and (b) oblique overpressure-time histories with dispersion correction applied to experimental results

It is immediately clear that the dispersion correction has effectively removed a large proportion of the oscillations in the experimental data, allowing for more accurate characterisation of peak overpressure. From the dispersion corrected normally reflected data it appears as though features such as the multiple shock front and subsequent pressure venting (from around 0.01 ms onwards) are in fact genuine features that are captured by the experimental setup. This gives confidence that the experimental approach is sufficient to (a) investigate the form of the near-field blast pressure load and (b) provide data for validation of numerical modelling approaches. Interestingly, although it is commonly believed that ConWep does not give accurate predictions at very short scaled distances, the ConWep predictions appear to be reasonably accurate as first-order estimations of the load the target will be subjected to.

The dispersion corrected experimental data suggests that the numerical approach may be simplifying the interaction between the shock front and the air/explosives interface. It is postulated by the current authors that turbulent mixing of the air and detonation products at the interface may lessen the magnitude of the multiple shock front, as the interface may comprise a more gradual density gradient than is modelled in the ALE analysis.

Importantly, however, the experimental methodology detailed herein enables more fundamental research of near-field blast loading to be carried out. The temporal and spatial resolution of the measured blast pressure allows analysts to be more rigorous and detailed with validation of numerical modelling approaches. It is suggested, therefore, that numerical and experimental research should be conducted simultaneously in order to better understand physical effects, rather than simply using experiments to ‘benchmark’ numerical results.

7. SUMMARY

It has been shown that an arrangement of Hopkinson pressure bars located in an effectively rigid target are capable of measuring the spatial and temporal blast pressure acting on a target subjected to an extremely close-in explosion. This method has distinct advantages over current experimental techniques: it is more robust and allows for larger pressures to be measured when compared to pressure gauges; and it allows for full temporal resolution of the load when compared to simple impulse plug methods.

Pressure-time recordings are presented for a 100 g sphere of PE4 detonated at 75 mm normal distance from the rigid target plate. Numerical analyses are conducted using LS-DYNA and the model is shown to be in good agreement with the experimental measurements, with the numerical impulse closely matching the experimentally recorded impulse.

Salient features of the near-field load are investigated. Evidence is provided for the existence of successive shock wave reflections off the air and detonation products contact interface. Localised clearing is also shown to occur, originating from the centre of the target and causing pressure equalisation and lateral velocities to act along the target face.

Experimental results are corrected for the effects of dispersion of the propagating waves in the pressure bars. The dispersion corrected experimental readings suggest that the features of near-field loading witnessed in the numerical model appear to be genuine. Such features mean that the traditional model of an exponential ‘Friedlander’ decay may be inaccurate for the temporal representation of near-field explosive events, although ConWep pressure and impulse predictions appear to be accurate as a first-order approach.

Work conducted in this paper suggests that numerical and experimental research should be conducted simultaneously in order to better understand physical effects.

ACKNOWLEDGEMENTS

The authors would like to express their gratitude to technical staff at Blastech Ltd. for their assistance in conducting the experimental work reported herein. The authors also wish to thank the Defence Science and Technology Laboratory for funding the published work.

REFERENCES

- [1] E. Esparza. Blast measurements and equivalency for spherical charges at small scaled distances. *International Journal of Impact Engineering*, 4(1):23–40, 1986.
- [2] C. N. Kingery and G. Bulmash. *Airblast parameters from TNT spherical air burst and hemispherical surface burst*. ARBRL-TR-02555, U.S Army BRL, Aberdeen Proving Ground, MD, USA, 1984.
- [3] US Department of Defence. *Structures to resist the effects of accidental explosions*. US DoD, Washington DC, USA, UFC-3-340-02, 2008.
- [4] D. W. Hyde. *Conventional Weapons Program (ConWep)*. U.S Army Waterways Experimental Station, Vicksburg, MS, USA, 1991.
- [5] G. Randers-Pehrson and K.A. Bannister. *Airblast loading model for DYNA2D and DYNA3D*. ARL-TR-1310, U.S Army Research Laboratory, Aberdeen Proving Ground, MD, USA, 1997.
- [6] J. O. Hallquist. *LS-DYNA Theory Manual*. Livermore Software Technology Corporation, CA, USA, 2006.
- [7] D. D. Rickman and D. W. Murrell. Development of an improved methodology for predicting airblast pressure relief on a directly loaded wall. *Journal of Pressure Vessel Technology*, 129(1):195–204, 2007.
- [8] A. Tyas, J. Warren, T. Bennett and S. Fay. Prediction of clearing effects in far-field blast loading of finite targets. *Shock Waves*, 21(2):111–119, 2011.
- [9] S. E. Rigby, A. Tyas, S. D. Fay, S. D. Clarke and J. A. Warren. Validation of semi-empirical blast pressure predictions for far field explosions – is there inherent variability in blast wave parameters? In: *6th International Conference on Protection of Structures against Hazards*, Tianjin, China, 2014.
- [10] K. Cheval, O. Loiseau and V. Vala. Laboratory scale tests for the assessment of solid explosive blast effects. Part I: Free-field test campaign. *Journal of Loss Prevention in the Process Industries*, 23(5):613–621, 2010.
- [11] K. Cheval, O. Loiseau and V. Vala. Laboratory scale tests for the assessment of solid explosive blast effects. Part II: Reflected blast series of tests. *Journal of Loss Prevention in the Process Industries*, 25(3):436–442, 2012.
- [12] D. Bogosian, J. Ferritto and Y. Shi. Measuring uncertainty and conservatism in simplified blast models. In: *30th Explosives Safety Seminar*, pages 1–26. Atlanta, GA, USA, 2002.
- [13] S. E. Rigby, A. Tyas, S. D. Clarke, S. D. Fay, J. A. Warren, I. Elgy and M. Gant. Testing apparatus for the spatial and temporal pressure measurements from near-field free air explosions. In: *6th International Conference on Protection of Structures against Hazards*, Tianjin, China, 2014.
- [14] D. H. Edwards, G. O. Thomas, A. Milne, G. Hooper and D. Tasker. Blast wave measurements close to explosive charges. *Shock Waves*, 2:237–243, 1992.

- [15] D. Cormie, W.P. Wilkinson, J. Shin and A.S. Whittaker. Scaled-distance relationships for close-in detonations. In: *15th International Symposium on the Interaction of the Effects of Munitions with Structures (ISIEMS)*. Potsdam, Germany, 2013.
- [16] W. P. Wilkinson, D. Cormie, J. Shin and A.S. Whittaker. Modeling close-in detonations in the near-field. In: *15th International Symposium on the Interaction of the Effects of Munitions with Structures (ISIEMS)*. Potsdam, Germany, 2013.
- [17] S. K. Hashemi and M. A. Bradford. Numerical Simulation of Free-Air Explosion Using LS-DYNA. *Applied Mechanics and Materials*, 553:780–785, 2014.
- [18] J. Shin, A. S. Whittaker, D. Cormie and W. Wilkinson. Numerical modeling of close-in detonations of high explosives. *Engineering Structures*, 81:88–97, 2014.
- [19] N. J. Huffington and W. O. Ewing. *Reflected impulse near spherical charges*. Technical Report BRL-TR-2678, Ballistic Research Laboratories, MD, USA, 1985.
- [20] M. W. Nansteel, R. L. Veldman, C. C. Chen and W. Lawrence. Impulse plug measurements of blast reflected impulse at close range. *Propellants, Explosives, Pyrotechnics*, 38(1):120–128, 2013.
- [21] S. Fay, S. Clarke, A. Tyas, J. Warren, S. Rigby, T. Bennett, I. Elgy and M. Gant. Measuring the spatial and temporal pressure variation from buried charges. In: *23rd International Symposium on the Military Aspects of Blast and Shock (MABS23)*. Oxford, UK, 2014.
- [22] S. D. Clarke, S. D. Fay, J. A. Warren, A. Tyas, S. E. Rigby and I. Elgy. A large scale experimental approach to the measurement of spatially and temporally localised loading from the detonation of shallow-buried explosives. *Measurement Science and Technology*, 26(1):015001, 2015.
- [23] M. Souli, A. Ouahsine and L. Lewin. ALE formulation for fluid-structure interaction problems. *Computer methods in applied mechanics and engineering*, 190:659–675, 2000.
- [24] B. Van Leer. Towards the ultimate conservative difference scheme. IV. A new approach to numerical convection. *Journal of Computational Physics*, 23:276–299, 1977.
- [25] E. L. Lee, H. C. Hornig and J. W. Kury. *Adiabatic expansion of high explosive detonation products*. TID 4500-UCRL 50422, Lawrence Radiation Laboratory, University of California, CA, USA, 1968.
- [26] B. M. Dobratz and P. C. Crawford. *LLNL explosives handbook - properties of chemical explosives and explosive simulants*. UCRL 52997, Lawrence Livermore National Laboratory, University of California, CA, USA, 1985.
- [27] S. E. Rigby, A. Tyas, T. Bennett, S.D. Fay, S.D. Clarke and J.A. Warren. A numerical investigation of blast loading and clearing on small targets. *International Journal of Protective Structures*, 5(3):253–274, 2014.
- [28] N. Aquelet and M. Souli. 2D to 3D ALE mapping. In: *10th International LS-DYNA Users Conference*, pages 23–34, Dearborn, MI, USA, 2008.
- [29] V. Lapoujade, N. Van Dorsselaer, S. Kevorkian and K. Cheval. A study of mapping technique for air blast modeling. In: *11th International LS-DYNA Users Conference*, pages 5–32, Detroit, MI, USA, 2010.
- [30] L. Schwer. A brief introduction to coupling Load Blast Enhanced with Multi-Material ALE: The best of both worlds for air blast simulation. In: *9th LS-DYNA Forum*, pages 1–12, Bamberg, Germany, 2010.
- [31] S. E. Rigby. *Blast wave clearing effects on finite-sized targets subjected to explosive loads*. PhD thesis, University of Sheffield, UK, 2014.
- [32] W. E. Baker. *Explosions in air*. University of Texas Press, Austin, TX, USA, 1973.
- [33] S. E. Rigby, A. Tyas, T. Bennett, J. A. Warren and S. Fay. Clearing effects on plates subjected to blast loads. *Engineering and Computational Mechanics*, 166(3):140–148, 2013.
- [34] S. E. Rigby, A. Tyas and T. Bennett. Single-degree-of-freedom response of finite targets subjected to blast loading – the influence of clearing. *Engineering Structures*, 45:396–404, 2012.
- [35] S. E. Rigby, A. Tyas and T. Bennett. Elastic-plastic response of plates subjected to cleared blast loads. *International Journal of Impact Engineering*, 66:37–47, 2014.
- [36] T. A. Rose and P. D. Smith. An approach to the problem of blast wave clearing on finite structures using empirical procedures based on numerical calculations. In: *16th Symposium on the Military Aspects of Blast and Shock (MABS16)*, pages 113–120. Oxford, UK, 2000.
- [37] Tyas A and Watson A. J. An investigation of frequency domain dispersion correction of pressure bar signals. *International Journal of Impact Engineering*, 25(1):87–101, 2001.